University of Tehran Press

Journal of the Earth and Space Physics

Homepage: https://jesphys.ut.ac.ir

Vol. 50, No. 4, Winter 2025, P. 115-124

(Research Article)

Investigating the Mechanism of Earthquakes in the Iranian Plateau Using the GCMT Catalogue

Rezapour, M.[1] ✉ | Rezaei, N.[1]

1. Department of Seismology, Institute of Geophysics, University of Tehran, Tehran, Iran.

Corresponding Author E-mail: rezapour@ut.ac.ir

(Received: 20 July 2024, Revised: 29 Oct 2024, Accepted: 4 Jan 2025, Published online: 15 March 2025)

Abstract

Routine estimates of the seismic moment (M_0) by the Global Centroid Moment Tensor Project (GCMT) for large and moderate earthquakes, provide a valuable resource for tectonic analysis. In this research, the source type of 614 earthquakes that occurred in the Iranian plateau between 1676 and 2023, whose moment tensor solutions are available in the GCMT catalogue, was investigated. Here, earthquakes are grouped according to dip angle values of the *T*, *P*, and *B* axes which were taken from GCMT catalogue. The mechanism is considered as strike-slip or normal faulting when the dip angle of the *B* or *P* axes exceeds 60°, respectively. When the dip angle of *T* axis exceeds 50°, the mechanism is proposed as thrust faulting. The focal mechanism study of 614 earthquakes showed that about 55.4, 25.4 and 2.9 percent of them have reverse, strike-slip and normal mechanisms, respectively. The average value equal to 0.12 for f_{CLVD} values of 614 earthquakes shows that the non-double-couple component in the deviatoric tensors is very small. Also, comparison of seismic moment estimated for 182 earthquakes by IRSC and GCMT, shows that there is an almost systematic bias in the seismic moment estimated by IRSC (Iranian Seismological Center). Seismic moment values reported by IRSC are lower than those determined by GCMT.

Keywords: Focal mechanism, Moment tensor, GCMT catalogue, Iranian plateau, IRSC.

1. Introduction

The formation of various Tethys basins, caused the fragmentation and separation of the supercontinents of Eurasia, Gondwana (~510 M years), blocks and subplates between them. In the Middle Cambrian Epoch, during the third stage of breaking apart from the most recent supercontinent of Pangaea (~335 M years) the Paleo-Tethys Ocean began to open (Zhai et al., 2015). The collision of the Indian and Asian plates in the Triassic period caused the closure of the Paleo-Tethys Ocean and the formation of the Alpine-Himalayan orogenic belt. The Iranian plateau is one of the most complex geodynamic settings within the Alpine-Himalayan orogenic belt, is a high land that includes a part of the Eurasian plate and a small part of the Arabian plate.

The plateau of Iran consists of several structural units, each of which has a relatively unique characteristic in terms of orogenic and tectonic events, stratigraphic and geological style. The Alborz and Zagros Mountain ranges form a large part of the Iranian plateau. The genesis of the rift during the main fracture of the Zagros is related to the creation of the Neotethys in the south and the closure of the Paleotethys in the north of Iran (Alborz Mountain range), which caused by the Hercynian orogeny phase in the Turan plate (Stöcklin, 1968). The PaleoThetys and NeoThetys ocean subduction are responsible for the formation several magmatic arcs and sedimentary basin zones within the Iranian plateau (Stampfli and Borel, 2002). These zones are separated from each other by thrust faults that display the ancient suture zones and ophiolite belts (Berberian and King, 1981; Richards, 2015).

The structural pattern and kinematics of active deformation in the region is controlled by a combination of interplaying tectonic forces governing over the Arabian–Eurasian convergence zone, due to extending a divergent boundary through the Red Sea and the Gulf of Aden (Figure 1). Therefore, the convergence of the Eurasian and Arabian plates causes deformation and earthquakes in the Iranian plateau. The deformation in northwest Iran is characterized by right-lateral

Cite this article: Rezapour, M., & Rezaei, N. (2025). Investigating the Mechanism of Earthquakes in the Iranian Plateau Using the GCMT Catalogue. *Journal of the Earth and Space Physics*, 50(4), 115-124. DOI: http//doi.org/10.22059/jesphys.2025.378399.1007613

E-mail: (1) rezaei.n@ut.ac.ir

Publisher: University of Tehran Press.
DOI: http//doi.org/10.22059/jesphys.2025.378399.1007613

Print ISSN: 2538-371X
Online ISSN: 2538-3906

movement at a velocity of 8 mm/year on the North Tabriz Fault, which is in agreement with the recurrence period of 250–300 years suggested by seismicity studies (Masson et al., 2006). Estimate deformation based on GPS and gravity observations in the Alborz Mountain range suggest that the eastern Alborz mainly accommodates strike slip deformation (~5 mm yr^{-1}), and that the western Alborz accommodates thrusting (~6 mm yr^{-1}) (Djamour et al., 2010). Also, the transversal NE trending shortening rate in the fold-and-thrust belt of Zagros increases from NW to SE and reaches about 10 mm yr^{-1} near its southeastern edge (Vernant et al., 2004). The velocity filed study in the Iranian plateau using GPS measurements by Mousavi et al. (2013) showed that the present-day northward motion decreases eastward from 11 mm yr^{-1} at Tehran (~52°E) to 1.5 mm yr^{-1} at Mashhad (~60°E), and N–S shortening across the Kopeh Dagh, Binalud and Koh-e-Sorkh ranges sums to 4.5±0.5 mm yr^{-1} at longitude 59°E.

Plotting the beach ball at the central location or another location on the map with an arrow connecting the beach ball and the epicenter is one of the most common ways to express earthquake focal mechanism. However it is difficult to show the mechanism of large number of earthquakes with different mechanisms by beach balls on map. A ternary plot or triangle plot is a barycentric plot on three variables. It graphically depicts the ratios of the three variables as positions in an equilateral triangle. It is used in different sciences such as petrology, mineralogy, etc. to show the compositional data in the three-dimensional case. Seismologists also use this diagram to display similarity and diversity of earthquake focal mechanisms. Triangle diagrams were first used to plot earthquake mechanisms by Apperson and Frohlich (1988) and Frohlich and Apperson (1992). Álvarez-Gómez (2019) used a ternary plot by presenting the software FMC (Earthquake focal mechanisms' data management, cluster, and classification). In this study, the mechanism of earthquakes occurred in the plateau of Iran is investigated using the triangular diagram and the Global Centroid Moment Tensor (GCMT) catalogue.

2. Data and processing

Global CMT catalogue was used in this study. One of the common methods of studying the geodynamics of a region is to determine the seismic moment tensor of earthquakes that occurred in that region. While the pioneering studies to determine the seismic moment occurred in the late 1960s and in the early 1970s, the Harvard CMT method of Dziewonski and Woodhouse (1983) became a common systematic determination of earthquake moment tensors.

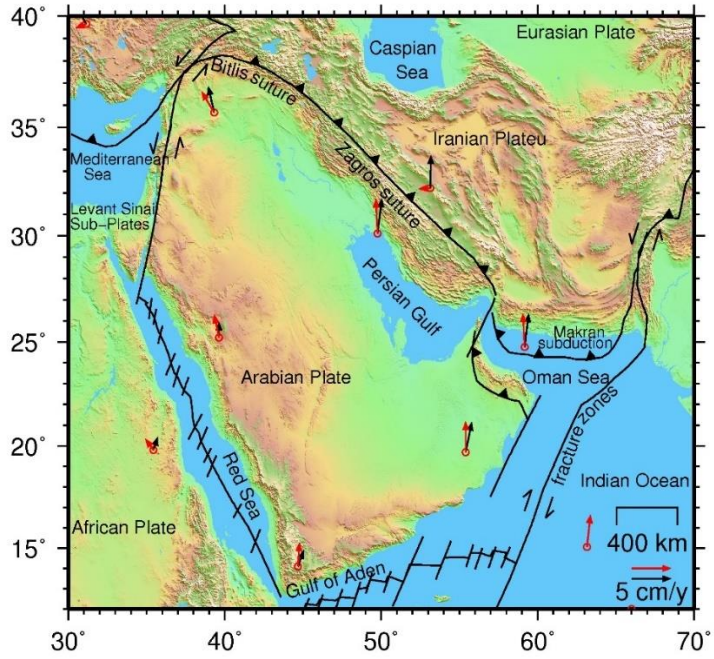

Figure 1. Tectonic map of the region, including major fault zones (black lines, after Al-Lazki et al., 2002). The red and black vectors present the absolute and relative motion of the plate, respectively (after, Al-Lazki et al., 2002).

Routine estimates of the seismic moment (M_0) by the Harvard group as Centroid Moment Tensor (CMT) solutions, developed and maintained as an extensive catalogue for most earthquakes above $m_b \approx 5.0$ over the period 1976-2006. Since then, it is maintained and continued by the Global Centroid Moment Tensor Project (GCMT) at the Lamont-Doherty Earth Observatory (LDEO) of Columbia University. The completeness of catalogue and accuracy vary both geographically and through time, and depend on earthquake depth and tectonic environment. The Harvard group has utilized long-period (45-200 sec) body and surface waves (for very large earthquakes) to determine scalar moments and moment tensors.

In the GCMT catalogue, for each earthquake, the available parameters are: origin time, epicentral coordinates, reported magnitude, data used in the CMT inversion, the type of source inverted for CMT, the type and duration of the moment-rate function assumed in the inversion; centroid parameters determined during the inversion, scalar moment value, moment-tensor elements, eigenvalues, plunge, and azimuth of the three eigenvectors, as well as the strike, dip, and rake of the nodal planes, among others. The moment tensor is specified by determining the trend and plunge of its *T*, *P*, and *B* axes (eigenvectors), and the values of its three principal moments (eigenvalues). The *T*, *P*, and *B* axes correspond to the principal axes associated with the largest, smallest, and intermediate principal moment values (m_T, m_P, m_B), respectively.

The source type can be determined using the orientation of the principal axes of the moment tensor. For earthquakes occurring on normal, reverse, and strike-slip faults, the *P*, *T*, and *B* axes oriented nearly vertically. Consequently, we have pure reverse mechanism when δ_T is 90°, a pure normal mechanism when δ_P is 90°, and a pure strike-slip mechanism when δ_B is 90° (Figure 2). In this figure, each beach ball plotted at the vertices of the triangle indicates a pure normal mechanism on a 45° dipping fault, a pure reverse mechanism on a 45° dipping fault, and a pure strike-slip mechanism on a vertical fault. In other words, the mechanisms triangle's vertices correspond to slip along the fault's strike or in the direction of the fault's slope. Other beach balls in Figure 2 illustrate faulting mechanisms that involve a combination of horizontal and vertical movement. The triangle diagram practically determine the fraction of dip-slip (reverse or normal) and strike-slip components of an earthquake.

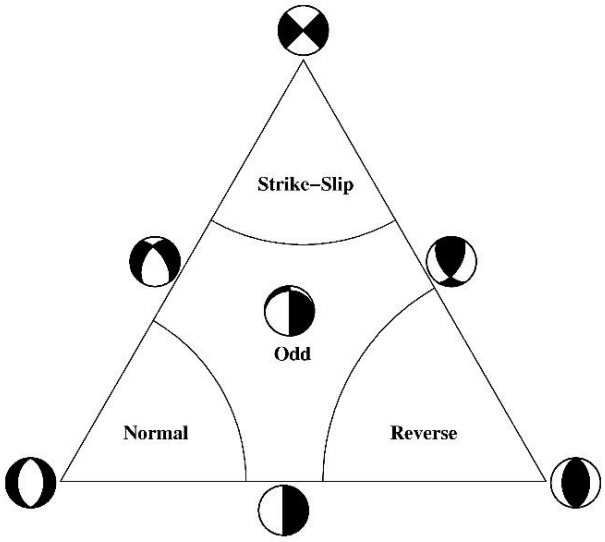

Figure 2. The three vertices correspond to pure normal, reverse, and strike-slip mechanisms. The curved lines in the figure correspond to mechanisms having *P* and *B* axes with dips of 60°, and a *T* axis with a dip to 50° (Frohlich and Apperson, 1992). For an earthquake with *T*, *P*, and *B* axes having dip angles relative to the horizontal of δ_T, δ_P, and δ_B, the proportions of the reverse, normal, and strike-slip mechanisms are $\sin^2 \langle\!\langle \delta_T \rangle\!\rangle$, $\sin^2 \langle\!\langle \delta_P \rangle\!\rangle$, and $\sin^2 \langle\!\langle \delta_B \rangle\!\rangle$, respectively. Therefore, we have $\sin^2 \langle\!\langle \delta_T \rangle\!\rangle + \sin^2 \langle\!\langle \delta_P \rangle\!\rangle + \sin^2 \langle\!\langle \delta_B \rangle\!\rangle = 1$, which is the equation of a sphere. Plotting the source mechanism on the triangle diagram is equivalent to the cartographer's problem of projecting locations from a quarter hemisphere onto a flat triangularsurface. This map projection is known as the azimuthal gnomonic projection (Richardus and Adler, 1972).

Earthquakes located within the latitude range of 24° to 40° and longitude range of 44° to 63° were extracted from the GCMT catalogue. In this way, 614 earthquakes that occurred between 1967 and 2023 were extracted. The researchers classified the earthquake mechanisms based on the plunge of the stress axes: *T*, *P*, and *B* (Frohlich and Apperson, 1992; Zoback, 1992; Johnson et al., 1994; Frohlich, 2001). Frohlich and Apperson (1992), Zoback (1992) and Johnson et al. (1994) classified the earthquake mechanisms into 4, 7 and 8 groups, respectively. Álvarez-Gómez (2019) utilized the classification from Johnson et al. (1994) in his FMC software. Therefore, the focal mechanism of an earthquake can be studied using the dip angles of eigenvectors ($\delta_T, \delta_P, \delta_B$).

Nouri-Delouei and Ghaitanchi (2021a, 2021b) studied the classification of earthquakes mechanisms in the Iranian plateau using FMC software. They classified the mechanisms of earthquakes into seven groups. Here, following the methodology of Frohlich and Apperson (1992), earthquakes are categorized into four groups according to dip angle values of the *T*, *P*, and *B* axes, which were taken from the GCMT catalogue. In Figure 3, the focal mechanisms of the 614 earthquakes are displayed on a triangle diagram. Figure 3 shows that both reverse and strike-slip mechanisms are common in the Iranian plateau, with reverse mechanisms predominating. About 55.4, 25.4 and 2.9 percent of all earthquakes shown in Figure 3 are classified as reverse, strike-slip, and normal mechanisms, respectively. Moreover, the remaining 16.3% of earthquakes have an odd mechanism, that is, a combination of the three mechanisms: reverse, strike-slip, and normal. The epicentral distribution of the 614 earthquakes is shown in Figure 4.

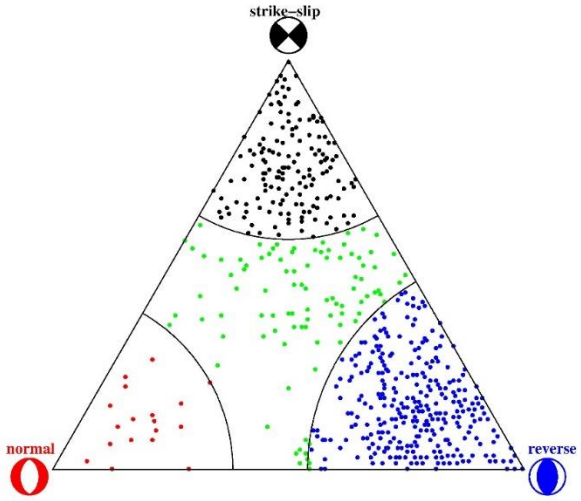

Figure 3. Triangle plot of extracted earthquakes from the GCMT catalogue. These earthquakes occurred in the Iranian Plateau between 1967 and 2023. In the set of 614 earthquakes, 340, 156, 18, and 100 earthquakes have reverse, strike-slip, normal, and odd mechanisms, respectively.

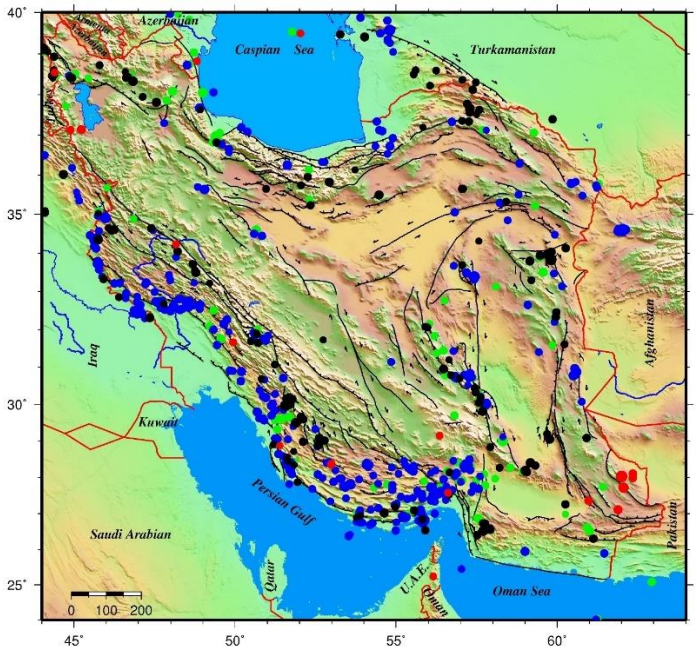

Figure 4. shows the spatial distribution of earthquakes. The blue, black, and red circles represent the epicenters of events with reverse, strike-slip and normal mechanisms. The green circles indicate events with odd mechanisms. All events are scaled according to their magnitudes. The solid lines show traces of major active faults in the region, as mapped by Hessami et al., 2003.

As anticipated, the earthquakes occurring in the Zagros Mountain range have a reverse mechanism. Due to the location of the Iranian Plateau within the Eurasian-Arabian Collision Zone, reverse mechanism earthquakes are predominant. While earthquakes with a strike-slip mechanism are also prevalent, those with a normal mechanism are quite rare. The occurrence of earthquakes with a combined mechanism shows the region's geodynamic complexity.

Histograms comparing hypocentral and centroid depth values for 614 selected earthquakes are presented in Figure 5. Hypocentral depth is determined using the arrival times of P and S phases, while centroid depth is determined by seismic wave inversion. The location of the hypocenter is at the point where the rupture is initiated, while the centroid is the location across the fault surface where slip is dominant. The centroid location coincided with the area where the maximum surface ruptures were observed. As shown in Figure 5, hypocentral depth values of 10 km and 33 km in the GCMT Catalogue are dominated by artificial effects, such as fixing for negative or unstable values, and probably as starting depths in the inversion routine. Similarly, centroid depth values of 12, 15, and 33 km are dominated by artificial effects. The values of 12 km, 15 km, and 33 km are probably corresponded to the average Conrad and Moho discontinuities. The routine GCMT procedures and algorithms are not expected to provide a depth resolution better than approximately 10–15 km for shallow earthquakes (Engdahl et al., 2006).

The seismic energy radiated from a fault can be modeled using a double-couple source, which serves as the equivalent body-force representation of the displacement field. A moment tensor with a nonzero isotropic component represents a change in volume. The moment tensor computed from seismic data may include contributions from other types of sources. It can be decomposed into isotropic and deviatoric parts, $M = M^I + M^D$. The deviatoric moment tensor is free of any isotopic sources but may contain an additional non-double-couple component, $M^D = M^{DC} + M^{CLVD}$. The non-double-couple component called *compensated linear vector dipoles* (*CLVDs*). These are sets of three force dipoles that are compensated, with one dipole -2 times the magnitude of the others. The trace of the *CLVD* is zero. Moment tensors estimated from waveform inversion rarely correspond to pure double couples. The estimated moment tensor can be decomposed into a major and minor double couple or into a major double couple and a *CLVD*. When there is a uniform inward/outward motion in a plane a *CLVD* source occurs, according to shortening/expansion normal to the plane.

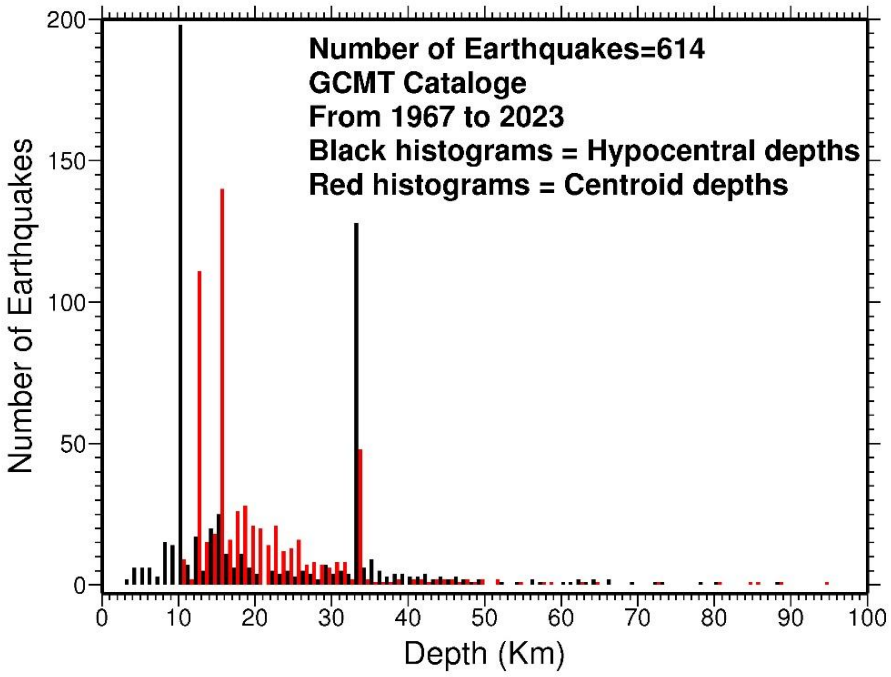

Figure 5. Histograms comparing hypocentral depths (black) with centroid depths (red) for 614 earthquakes in GCMT catalogue which occurred in the Iranian plateau.

We can identify the type of source by examining the eigenvalues of the moment tensor. In an ideal explosion, all eigenvalues are equal, and none are zero. In a double-couple source, two eigenvalues are equal in magnitude and opposite in sign, while the third is zero. Frohlich and Apperson (1992) proposed a method to express the non-double-couple component of moment tensors as follows:

$$f_{CLVD} = (min(|m_T|, |m_P|, |m_B|)) / max(|m_T|, |m_P|, |m_B|) = |m_B| / max(|m_T|, |m_P|) \quad (1)$$

where m_T, m_B and m_P are the largest, intermediate, and smallest principal moments, respectively. The f_{CLVD} i.e., compensated linear vector dipole ratio measures how different the source is from a pure double-couple source. The f_{CLVD} is equal to zero in a pure double-couple source and is equal to 0.5 in a pure *CLVD* source. We expect to observe a minor *CLVD* component in the inversion of the moment tensor due to inaccurate propagation corrections attributed to the noise. Some events have a *CLVD* value larger than expected to be caused by noise.

While the Harvard group, in their routine earthquake modeling, includes a constrain that the isotropic component equals zero for stability purposes, they do not constrain the CMT solutions to be pure double-couples (Ammon et al., 2021). Therefore, many earthquakes have a substantial *CLVD* component. Figure 5 shows the histogram of f_{CLVD} values for the 614 earthquakes that occurred in the Iranian plateau. The mean of f_{CLVD} values for these earthquakes in the CMT catalogue occurred in Iranian plateau is 0.12. Moment tensors from sources such as the opening of a crack under tension, the inflation of a magma dike in volcanic areas, deep earthquakes, and near-simultaneous earthquakes on adjacent faults with varying geometries have a large *CLVD* component, but they are rare. More than one physical mechanism is required to explain the observed varieties of non-double-couple earthquakes. The simplest explanation is that some earthquakes are complex, with stress released on two or more suitably oriented, nonparallel fault surfaces (Frohlich, 1994). The *CLVD* components reflect the complexities in the earthquake source, e.g., irregularly shaped faults, seismic anisotropy, shear-tensile faulting induced by fluid injection in volcanic or geothermal areas, or the presence of a material interface in the focal zone (Frohlich, 1994; Vavryčuk and Hrubcová, 2017).

In a deviatoric source, the deviation from a pure double-couple is given by the percentage of *CLVD* present, by the $200 \times f_{CLVD}$. For an earthquake with $f_{CLVD} = 0.25$, about 50% of its moment is *CLVD* component. As Figure 6 shows, only 12.4% of the used dataset has *CLVD* value greater than or equal to 0.25 in the estimated moment tensors.

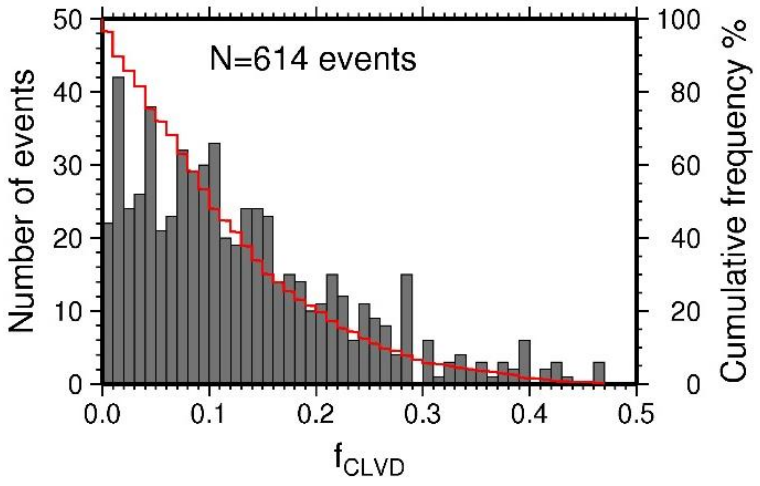

Figure 6. Histogram of f_{CLVD} values in bins with a width of 0.01, for earthquakes occurring between 1976 and 2023 in the Iranian plateau. A measure often quoted is $200 \times f_{CLVD}$, which is the percent non-double component. The red-line and the right axis present the cumulative frequency of f_{CLVD} values.

3. Comparison GCMT and IRSC catalogues

As mentioned before, the Harvard group reported Centroid Moment Tensor (CMT) solutions for earthquakes with $m_b \geq 5.0$, during 1976 to 2006. Since then, it is maintained and continued by the Global Centroid Moment Tensor Project (GCMT) at Columbia University. Iranian Seismological Center (IRSC) has been reporting the moment tensor solution for moderate and large earthquakes that have occurred in the Iranian plateau since 2012. IRSC applies the ISOLA, ISOLated Asperities software package (Sokos and Zahradník, 2008, 2013) to local and regional waveforms to perform the moment tensor inversion (Hosseini et al., 2019). Hosseini et al. (2019) published the seismic moments of 194 earthquakes as IRSC catalogue. They compared the seismic moments of 111 events in the IRSC and GCMT catalogues and concluded that the values of the seismic moments in the IRSC catalogue are underestimated compared to the values published in the GCMT catalogue. In this study, comparing IRSC and GCMT catalogues shows that for 182 earthquakes occurred in the Iranian plateau, their moment tensor solutions are available in both catalogues. Also, Ahmadzadeh and Javan (2024) recently published the focal mechanism of 64 earthquakes that occurred in Alborz region. They collected all available focal mechanism for which the quality of solutions could be determined in order to construct a focal mechanism catalogue for the Alborz region. Here, estimated source parameters such as the seismic moment, hypocentral and centroid depth are compared for two catalogues (Figure 7).

Figure 7 shows the comparison of seismic moment estimated by IRSC and GCMT. This figure indicates that there is an almost systematic bias in the seismic moment estimated by IRSC. Seismic moment values reported by IRSC are lower than those determined by GCMT. For this difference, various reasons such as the type of data (local, regional, or teleseismic), the velocity model (local or global), different frequency band, and incorrect seismometer response in the process of inversion can be mentioned. IRSC uses a local velocity model and local/regional data, while in the GCMT project the teleseismic data and the global velocity model of PREM (Dziewonski and Anderson, 1981) are used.

Also, the hypocentral and centroid depth reported in both catalogues are compared in Figure 8. As Figure 8a shows, hypocentral-depth value of 10 and centroid depth value of 12 km in the GCMT Catalogue are dominated by artificial effects. In the set of the 182 earthquakes that were compared, for 89 earthquakes, the GCMT reported a hypocentral depth value of 10 km. Besides, in this dataset the lowest centroid depth in the GCMT catalogue is 12 km, and this value has been reported for 49 earthquakes (Figure 8b). Figure 8b shows that the CMT depth tends to be larger than the IRSC depth. The source inversion process is sensitive to the various choices that must be made regarding dataset, earth model and inversion strategy. These observed discrepancies in the estimated depth values may be related to the Earth models that Harward group (CMT) and IRSC use in their depth determinations. In the CMT, the PREM model is used. IRSC uses a local structural velocity model.

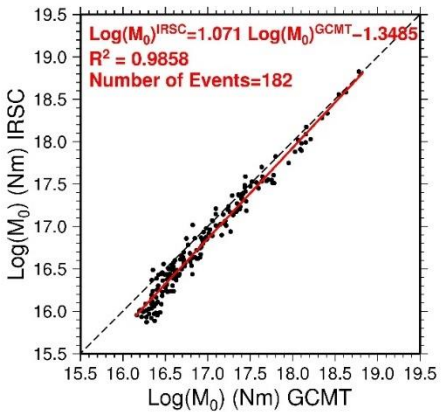

Figure 7. Relation between seismic moment values for the 182 earthquakes reported by IRSC and GCMT from 2012 to 2023. The regression line is shown by a red line.

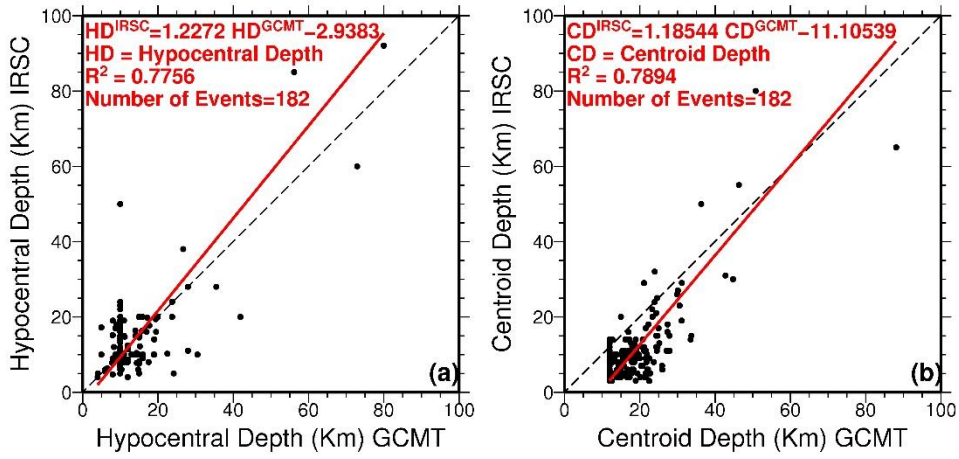

(a) (b)

Figure 8. Relation between depth values for the 182 earthquakes reported by IRSC and GCMT from 2012 to 2023. (a) For hypocentral depth. (b) For centroid depth. In each case, the regression line is shown by a red line. R = correlation coefficient.

4 Conclusion

In this paper, we applied the ternary plot to evaluate the distribution of focal mechanism orientations of groups of earthquakes. The method was applied to 614 earthquakes that occurred in the Iranian plateau between 1976 and 2023, whose moment tensor solutions are available in the GCMT catalogue. Here, following Frohlich and Apperson (1992), the source type of earthquakes grouped according to dip angle values of the *T*, *P*, and *B* axes taken from GCMT catalogue. The applied method demonstrates that 55.4, 25.4 and 2.9 percent of earthquakes have reverse, strike-slip, and normal mechanisms; however, there is a significant portion (16.3 %) that have mechanisms, which plot in the center of the triangle diagram, well away from the reverse, strike-slip, or normal vertices (Figure 3).

While the routine earthquake modeling in the Global Centroid Moment Tensor Project (GCMT), due to stability of modeling, include a constraint that the isotropic component equals zero, the CMT solutions are not constrained to be pure double-couples. Therefore, many earthquakes have a substantial *CLVD* component. Among the best determined 614 moment tensors for earthquakes in the Iranian plateau, only 12.4% has *CLVD* value greater than or equal to 0.25.

Also, comparison of the seismic moment estimated for the 182 earthquakes by IRSC and GCMT, shows that there is an almost systematic bias in the seismic moment estimated by IRSC. Seismic moment values reported by IRSC are lower than those determined by GCMT.

Acknowledgment

All data used in this study were extracted from websites of seismological centres: Iranian Seismological Centre (IRSC); Global Centroid Moment Tensor (GCMT). The authors are grateful for their contributions to this research. The figures were prepared using Generic Mapping Tools (Wessel and Smith, 1998).

References

Ahmadzadeh, S., & Javan-Doloei, Gh. (2024). The high-frequency decay parameter Kappa (κ) in the Alborz Region using broadband seismic waveforms. *Journal of Seismology*. 1-18. 10.1007/s10950-024-10256-x.

Ammon, C.J., Velasco, A.A., Lay, T., & Wallace, T. (2021). Foundations of Modern Global Seismology, Elsevier, Academic Press.

Al-Lazki, A., Seber, D., & Sandvol, E. (2002). A crustal transect across the Oman Mountains on the eastern margin of Arabia. *GeoArabia*, 7, 47-78.

Álvarez-Gómez, J. A., (2019). FMC—Earthquake focal mechanisms data management, cluster and classification. *SoftwareX*, 9, 299-307.

Apperson, K. D., & Frohlich, C. (1988). The effect of the plate boundary on average earthquake focal mechanisms in convergent margins, *Geol. Soc., Abstr.*

Programs, 20, A236.

Berberian, M., & King, G.C.P. (1981). Towards a paleogeography and tectonic evolution of Iran. *Can. J. Earth Sci.* 18, 210–265.

Engdahl E.R., Jackson J.A., Myers S.C., Bergman E.A., & Priestley K. (2006). Relocation and assessment of seismicity in the Iran region, *Geophys. J. Int.*, 167, 761–778.10.1111/j.1365-246X.2006. 03127.x

Dziewonski, A.M., & Anderson, D.L., (1981). Preliminary reference Earth model. *Phys. Earth Planet. Inter.* 25 (4), 297–356.

Dziewonski, A. M., & Woodhouse, J.H. (1983). An experiment in systematic study of global seismicity: Centroid-moment tensor solutions for 201 moderate and large earthquake of 1981, *J. Geophys. Res., 88,* 3247-3271.

Djamour, Y., Vernant, P., Bayer, B., Nankali, H.R., Ritz, J.F., Hinderer, J., Hatam, Y., Luck, B., Moigne, L.N., Sedighi, M., & Khorrami, F. (2010) GPS and Gravity Constraints on Continental Deformation in the Alborz Mountain Range, Iran. *Geophys. J. Int*, 183, 1287-1301. https://doi.org/10.1111/j.1365-246X.2010.04811.x

Frohlich, C. (1992). Triangle diagrams ternary graphs to display similarity and diversity of earthquake focal mechanisms. *Phys Earth Planet Inter*, 75 193-198.

Frohlich, C. (1994) Earthquakes with non-double-couple mechanisms, *Science*, 264(5160), 804-809.

Frohlich, C., & Apperson, K. D. (1992). Earthquake focal mechanisms, moment tensors, and the consistency of seismic activity near plate boundaries. *Tectonics*, 11 279-296.

Hessami, K., Jamali, F., & Tabassi, H. (2003). Major active faults of Iran, scale 1:25,000,000. Ministry of Science, Research and Technology, International Institute of Earthquake Engineering and Seismology, Iran.

Hosseini, H., Pakzad, M., & Naserieh, S., (2019). Iranian regional centroid moment tensor catalogue: Solutions for 2012–2017. *Phys. Earth Planet. Inter*., 286, 29-41.

Masson, F., Djamour, Y., Van-Gorp, S., Chery, J., & Tatar, M., Tavakoli, F., Nankali, H. and Vernant, P. (2006). Extension in NW Iran driven by MW 6.5, 6.4 Ahar-Varzghan doublet earthquakes 1203 the motion of the South Caspian Basin. *Earth and Planetary Science Letters,* 252, 180–188.

Mousavi, Z., Walpersdorf, A., Walker, R.T., Tavakoli, F., Pathier, E., Nankali, H., Nilfouroushan., F., & Djamour, Y. (2013). Global Positioning System constraints on the active tectonics of NE Iran and the South Caspian region, *Earth and Planetary Science Letters,* 377-378, 287–298.

Nouri-Delouei, M., & Gheitanchi, M.R., (2021a). Fault mechanisms and their frequencies during destructive earthquakes in Iran. *Tectonics Journal*, 5, 91-102.

Nouri-Delouei, M., & Gheitanchi, M.R., (2021b). Classification of Zagros earthquakes based on focal mechanism. *Contributions to Geophysics and Geodesy*, 51, 265-275.

Richards, J.P. (2015) Tectonic, magmatic, and metallogenic evolution of the Tethyan orogen: From subduction to collision, *Oro Geology Reviews*, 70, 323-345.

Richardus, P., & Adler, R.K. (1972). Map Projections North Holland, Amsterdam, 174 pp.

Stöcklin, J. (1968). Structural history and tectonics of Iran, a review, *Am. Assoc. Pet. Geol. Bull*., 52, 1229–1258.

Stampfli, G.M., & Borel, G.D. (2002). A plate tectonic model for the Paleozoic and Mesozoic constrained by dynamic plate boundaries and restored synthetic oceanic isochrons. *Earth Planet. Sci. Lett.* 196, 17–33.

Sokos, E., & Zahradník, J. (2008). ISOLA – A Fortran code and a Matlab GUI to perform multiple-point source inversion of seismic data, *Comput. Geosci*., 34, 967–977.

Sokos, E., & Zahradník, J. (2013). Evaluating Centroid-Moment-Tensor Uncertainty in the New Version of ISOLA Software, *Seismological Research Letters*, 84, 656-665.

Vavryčuk, V., & Hrubcová, P. (2017) Seismological evidence of fault weakening due to erosion by fluids from observations of intraplate earthquake swarms, *J. Geophys. Res*., 122, doi.org/10.1002/2017JB013958.

Vernant, P., Nilforoushan, F., Hatzfeld, D., Abbasi, M. R., & Vigny, C. (2004). Contemporary crustal deformation and plate kinematics in Middle East constrained by GPS measurements in Iran

and northern Oman. *Geophys. J. Int*, 157, 381–398.

Zhai, Q. G., Jahn, B. M., Wang, J., Hu, P. Y., Chung, S. L., Lee, H. Y., Tang, S. H., & Tang, Y. (2015). Oldest Paleo-Tethyan ophiolitic mélange in the Tibetan Plateau. *Geological Society of America Bulletin.* 128 (B31296-1): 355–373. doi:10.1130/B31296.1.

Zoback, M.L., (1992). Stress Field Constraints on Intraplate Seismicity in Eastern North America. *J. Geophys. Res*. 92, 11761-11782.